Algebraic Dynamic Multilevel (ADM) Method for Immiscible Multiphase Flow in Heterogeneous Porous Media with Capillarity

Cusini, Matteo; van Kruijsdijk, Cor; Hajibeygi, Hadi

Publication date
2016

Document Version
Final published version

Published in
15th European Conference on the Mathematics of Oil Recovery

EAGE

ECMOR XV

We Gra 16

Algebraic Dynamic Multilevel (ADM) Method for Immiscible Multiphase Flow in Heterogeneous Porous Media with Capillarity

M.C. Cusini* (TU Delft), C. van Kruijsdijk (Shell) & H. Hajibeygi (TU Delft)

SUMMARY

An algebraic dynamic multilevel method (ADM) is developed for fully-implicit (FIM) simulations of multiphase flow in heterogeneous porous media with strong non-linear physics. The fine-scale resolution is defined based on the heterogeneous geological one. Then, ADM constructs a space-time adaptive FIM system on a dynamically defined multilevel nested grid. The multilevel resolution is defined using an error estimate criterion, aiming to minimize the accuracy-cost trade-off. ADM is algebraically described by employing sequences of adaptive multilevel restriction and prolongation operators. Finite-volume conservative restriction operators are considered whereas different choices for prolongation operators are employed for different unknowns. The ADM method is applied to challenging heterogeneous test cases with strong nonlinear heterogeneous capillary effects. It is illustrated that ADM provides accurate solution by employing only a fraction of the total number of fine-scale grid cells. ADM is an important advancement for multiscale methods because it solves for all coupled unknowns (here, both pressure and saturation) simultaneously on arbitrary adaptive multilevel grids. At the same time, it is a significant step forward in the application of dynamic local grid refinement techniques to heterogeneous formations without relying on upscaled coarse-scale quantities.

Introduction

Accurate numerical simulations of complex multiphase flow processes in porous media often require much finer grid resolutions than those commonly used by the state-of-the-art reservoir simulators. The reason is that many complex multiphase phenomena (e.g. viscous fingering (Homsy, 1987), phase splitting and mass transfer between phases) take place at length scales that are significantly smaller than the sizes of natural formations. In addition to this, geological properties (e.g. permeability and porosity) are heterogeneous with high resolutions (fine scale) over the entire large length scales of the subsurface reservoir. Unfortunately, the number of grid cells required to capture all these complexities would require the solution of linear systems that cannot be handled efficiently with today's computational power. For this reason, advanced simulation methods have to be developed to reduce the computational cost without affecting significantly the accuracy of the solution.

One of the methods used to overcome this issue is the dynamic local grid refinement (DLGR) technique. This technique relies on the local nature of many physical interactions and dynamically adjusts the grid resolution throughout the domain. This way, high-resolution grids are employed only in a small fraction of the domain with a considerable reduction of the number of degrees of freedom. DLGR techniques were introduced and evolved in reservoir simulation since the 1980s (Bell and Shubin, 1983; Berger and Oliger, 1984; Heinemann et al., 1983; Han et al., 1987; Schmidt and Jacobs, 1988; Nilsson et al., 2005; Edwards and Christie, 1993). Different DLGR methods have been developed for both finite-element (FE) and finite-volume (FV) methods and for both sequential (Pau et al., 2012) and fully implicit (FIM) (Boerrigter et al., 2011) simulation strategies. Recent advancements have also shown their applicability to more complex physics (Faigle et al., 2014; Jackson et al., 2015), including multiphase flows with compositional effects (Boerrigter et al., 2011).

Most DLGR techniques developed so far were designed mainly for homogeneous reservoirs. However, natural formations present heterogeneous geological properties that have a great impact on the resulting flow path. Crossing the scales for highly heterogeneous media is very challenging as geological properties have to be defined at different resolutions. The few proposed methods in the literature (see e.g. (Hoteit and Chawathé, 2014)) aim to describe a flow-based upscaling technique to generate single-phase effective properties at different resolutions, which is used later during simulation whenever needed. It is important to note that only multiscale methods (Jenny et al., 2003) allow for systematic mapping between both fine and coarse levels, using locally solved and adaptively updated basis functions (Hajibeygi and Jenny, 2011; Kunze et al., 2013; Zhou et al., 2011).

Recently, an Algebraic Dynamic Multilevel (ADM) method (Cusini et al., 2016) was proposed for multiphase flow in heterogeneous porous media. The ADM extended the applicability of multiscale methods in the sense that it was employed to FIM systems, where all unknowns crossed multiple scales. At the same time, it was a significant step forward for DLGR methods, as it was describing an algebraic framework applicable to heterogeneous transmissibility fileds with no dependency on upscaled coarse quantities. ADM could be applied to FIM and sequential-implicit coupling approaches, allowing for full flexibility in terms of non-linear coupling enhancements.

Although ADM was found efficient for many practical water-flood test cases with highly heterogeneous permeability fields, the real-field applications include much stronger non-linear physics. Of great importance is to extend the ADM formulation and methodology to include strongly non-linear capillary effects (Chaouche et al., 1994; Helmig et al., 2007; Li, 2014) which impose significant challenges to simulators.

In this paper, the ADM method is successfully extended to include heterogeneous reservoirs with increasing level of non-linear heterogeneous capillary effects. For all cases considered here, the ADM solutions are compared against fine-scale reference results. It is shown that ADM provides an accurate solution by employing only a small fraction of the fine-scale grid blocks. The evolution of the number of grid-blocks is also presented along with the sensitivity of the ADM solution to the coarsening criterion used.

The paper is organized as follows: next, the governing equations and the fine-scale discretization scheme are briefly described. Then, ADM method for scenarios with non-linear physics is presented. This section is followed by a section on numerical results, where the efficiency and applicability of the method is studied. The paper is concluded at the end.

Governing equations and fine-scale discrete system

Mass conservation equation for phase α of total N_α immiscible phases flowing through a porous medium reads

$$\frac{\partial(\phi S_\alpha)}{\partial t} - \nabla \cdot (\lambda_\alpha \cdot \nabla p_\alpha) - q_\alpha = 0 \quad \forall \alpha \in \{1,...,N_\alpha\}, \tag{1}$$

where ϕ is the porosity, S_α, p_α and q_α are the saturation, pressure and source terms of phase α. Moreover, λ_α is the phase mobility defined as $\lambda_\alpha = \mathbf{K}\frac{k_{r\alpha}}{\mu_\alpha}$ where $\mathbf{K}$ is the rock permeability tensor, $k_{r\alpha}$ and μ_α are, respectively, the relative permeability and the viscosity of phase α. Note that Darcy's law is used to relate phase velocity with phase pressure gradient, i.e., $u_\alpha = -\lambda_\alpha \cdot \nabla p_\alpha$.

For a two phase system, phase pressures can be related through capillary pressure (P_c) function, i.e.

$$P_w = P_{nw} - P_c, \tag{2}$$

where the subscripts w and nw indicate the wetting and the non-wetting phases, respectively. In its most generic form, capillary pressure is a function of both rock properties and of the wetting phase saturation (Brown, 1951; Leverett, 1941) (S_w), i.e.

$$P_c = \sigma cos(\theta)\sqrt{\frac{\phi}{K}}J(S_w), \tag{3}$$

where

$$J(S_w) = C_1\left(\frac{1-S_{wirr}}{S_w - S_{wirr}}\right)^{C_2}. \tag{4}$$

Here, σ is the surface tension, θ is the contact angle, C_1 and C_2 are two constants characterizing the fluid and the geological properties of the formation, and $S_{w_{irr}}$ is the irreducible wetting phase saturation. The N_α mass conservation equations (Eq. (1)) along with the proper boundary conditions, the constraint $\sum_{\alpha=1}^{N_\alpha} S_\alpha = 1$ and the capillary relationships between all phase pressures, form a well-posed problem of $N_\alpha + 1$ unknowns. The saturation constraint can be used to eliminate one equation, resulting in a system of N_α unknowns, i.e., one phase pressure and $N_\alpha - 1$ phase saturations. This system of equations is solved numerically by applying an implicit and a finite volume (FV) scheme in time and space, respectively. Thus, all pressure- and saturation-dependent terms are evaluated at the new time-step $n+1$ and the residual function is set to be equal to zero, i.e.

$$r_\alpha^{n+1} = \frac{\phi}{\Delta t}(S_\alpha^{n+1} - S_\alpha^n) - \nabla \cdot (\lambda_\alpha^{n+1} \cdot \nabla(p_1^{n+1} + (1-\delta_{1\alpha})P_{c_\alpha}^{n+1})) - q_\alpha^{n+1} = 0 \quad \forall \alpha \in \{1,...,N_\alpha\}, \tag{5}$$

where $\delta_{1\alpha}$ is the Dirac delta ($\delta_{1\alpha} = 1$ only if $\alpha = 1$, i.e. the first phase is the most wetting phase).
Since the residual is a non-linear function of the primary variables a Newton-Raphson method has to be employed to solve iteratively the system of equations. The residual at iteration level $\nu+1$ is approximated as

$$r_\alpha^{\nu+1} \approx r_\alpha^\nu + \left.\frac{\partial r_\alpha}{\partial p_1}\right|^\nu \delta p_1^{\nu+1} + \left.\frac{\partial r_\alpha}{\partial S_\beta}\right|^\nu \delta S_\beta^{\nu+1} \quad \forall \alpha \in \{1,...,N_\alpha\} \quad \text{and} \quad \forall \beta \in \{2,...,N\}. \tag{6}$$

Thus, a linear system $\mathbf{J}_f^\nu \delta x_f^{\nu+1} = -r_f^{\nu+1}$ is solved at each Newton-Raphson iteration. Here, δx_f is the vector of unknowns, $\mathbf{J}_f^\nu$ is the derivatives (Jacobian) matrix and r_f^ν is the residual vector. Finally, the

linear system for N_α phases, where the pressure of phase 1 and the remaining $N_\alpha - 1$ saturation are chosen as primary unknowns, reads

$$\underbrace{\begin{pmatrix} J^\nu_{1p} & \cdots & J^\nu_{1S_{N_\alpha-1}} \\ \vdots & \ddots & \vdots \\ J^\nu_{N_\alpha p} & \cdots & J^\nu_{N_\alpha S_{N_\alpha-1}} \end{pmatrix}}_{\mathbf{J}^\nu_f} \underbrace{\begin{pmatrix} \delta p^{\nu+1} \\ \vdots \\ \delta S^{\nu+1}_{N_\alpha-1} \end{pmatrix}}_{\delta x^{\nu+1}_f} = - \underbrace{\begin{pmatrix} r^\nu_1 \\ \vdots \\ r^\nu_{N_\alpha} \end{pmatrix}}_{r^\nu_f}. \tag{7}$$

Each row of the matrix $\mathbf{J}^\nu_f$ corresponds to the mass conservation equation of phase α, with N_α columns corresponding to the primary unknown variables.

Algebraic Dynamic Multilevel (ADM) method

The ADM method provides a high-quality approximate solution for Eq. (7), which captures important physical interactions involved in the process, on an adaptive dynamic grid resolution. A hierarchy of nested n_l-level coarse grids is built on top of the N_f fine-scale cells. At each time-step, ADM defines a solution grid by combining previously-defined cells belonging to the $(n_l + 1)$ levels (n_l coarse- and 1 fine-scale) with a total of $N^{ADM}_l << N_f$ grid cells (see fig. 1). The grid resolution is chosen based on an error criterion (here, the difference in saturation between two neighboring cells) that ensures fine-scale resolution is only used in subregions with steep solution gradients. Note that static fine-scale resolution is employed around the wells. In addition, the resolution change between two neighboring grid-blocks is limited to one level.

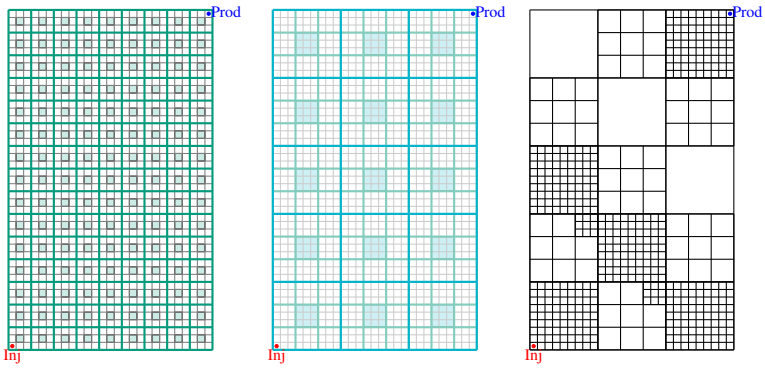

(a) coarse level 1 (b) coarse level 2 (c) ADM solution grid

Figure 1 *2-level ADM method: coarse grids on level 1 (a) and level 2 (b), for a coarsening ratio equal to 3, and (c) the ADM solution grid for $n_l = 2$.*

ADM is based on the assumption that the solution on the fine-scale grid can be approximated by

$$\delta x_f \approx \prod_{l=1}^{n_l} \hat{\mathbf{P}}^l_{l-1}\, \delta x_{n_l}, \tag{8}$$

where $\hat{\mathbf{P}}^l_{l-1}$ is the prolongation operator between the ADM grid on level l and $l-1$. On the other hand, the discretized equations on level l can be mapped to a coarser ADM resolution $l+1$ by applying the restriction operator $\hat{\mathbf{R}}^l_{l+1}$. Thus, the ADM coarse system $\mathbf{J}^{ADM}_{n_l} \delta x_{n_l} = -r^{ADM}_{n_l}$ is constructed by applying a sequence of restriction and prolongation operators, i.e.

$$\underbrace{\hat{\mathbf{R}}^{n_l}_{n_l-1} \cdots \hat{\mathbf{R}}^1_f \mathbf{J}_f \hat{\mathbf{P}}^f_1 \cdots \hat{\mathbf{P}}^{n_l-1}_{n_l}}_{\mathbf{J}^{ADM}_{n_l}} \delta x_{n_l} = - \underbrace{\hat{\mathbf{R}}^{n_l}_{n_l-1} \cdots \hat{\mathbf{R}}^1_f r_f}_{r^{ADM}_{n_l}} \tag{9}$$

Note that all $\hat{\mathbf{R}}_l^{l-1}$ and $\hat{\mathbf{P}}_{l-1}^{l}$ operators are block matrices of the form

$$\hat{\mathbf{R}}_l^{l-1} = \begin{pmatrix} \hat{R}_l^{l-1} & 0 & 0 \\ 0 & \ddots & 0 \\ 0 & 0 & \hat{R}_l^{l-1} \end{pmatrix} \quad \text{and} \quad \hat{\mathbf{P}}_{l-1}^{l} = \begin{pmatrix} \hat{P}_{l-1_p}^{l} & 0 & 0 \\ 0 & \ddots & 0 \\ 0 & 0 & \hat{P}_{l-1_{S_{N_\alpha-1}}}^{l} \end{pmatrix}, \tag{10}$$

where the number of rows of $\hat{\mathbf{R}}_l^{l-1}$ and $\hat{\mathbf{P}}_l^{l-1}$ is equal to the number of primary variables. The blocks $\hat{R}_l^{l-1}$ are finite volume restriction operators, $N_l^{ADM} \times N_{l-1}^{ADM}$, that ensure mass conservation at all levels, i.e.

$$\hat{R}_l^{l-1}(i,j) = \begin{cases} 1 & \text{if finer cell j is inside coarser cell i} \\ 0 & \text{otherwise} \end{cases} \tag{11}$$

The blocks $\hat{P}_{l-1}^{l}$ are, instead, matrices of size $N_{l-1}^{ADM} \times N_l^{ADM}$ and their columns contain the interpolators of the corresponding variable. Consequently, different interpolators can be used for each variable. In this paper multiscale basis functions (Hou and Wu, 1997; Jenny et al., 2003) are considered as pressure interpolators whereas constant interpolation is employed for saturation unknowns (fig. 2). A more detailed description of the sequence of prolongation and restriction operators can be found in Cusini et al. (2016).

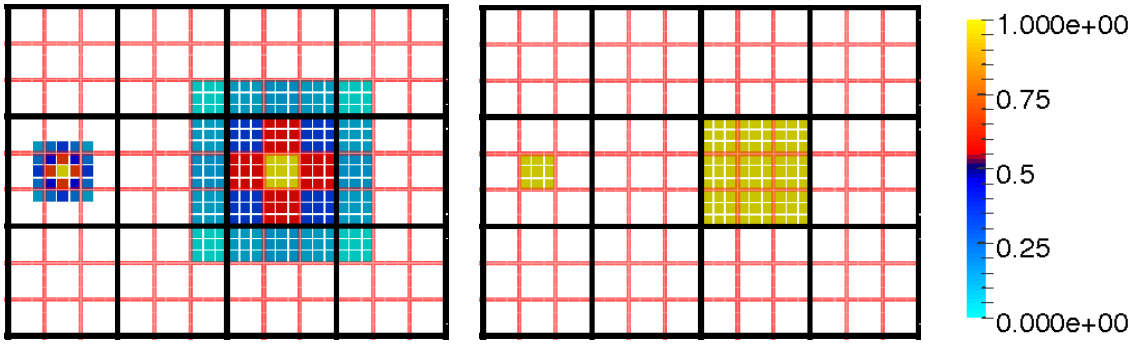

(a) Pressure (b) Saturation

Figure 2 *2-level ADM method: interpolators for pressure (a) and saturation (b). A multiscale basis function (here for a homogeneous reservoir) is used for pressure whereas constant interpolation is employed for saturation variables. A basis function for both the first and the second coarse levels are shown.*

An overview of the ADM procedure for one time-step is presented in Algorithm 1. Note that non-linear convergence is always reached on the ADM resolution (in terms of the norm of r_l^{ADM} and of δx_l) and that the grid resolution is chosen explicitly (e.g., for time-step $n+1$ the grid resolution is chosen based on the solution at time-step n). For this reason, some extra refinement is introduced ahead of the moving saturation front as a “safety margin".

Algorithm 1: ADM method solution algorithm for one time-step.

Data: Solution at previous time-step.
Result: Solution at current time-step.
Initialize time-step;
Compute fine-scale residual r_f;
Select grid resolution;
Construct sequences of $\hat{\mathbf{R}}$ and $\hat{\mathbf{P}}$;
Restrict fine-scale residual:
$r_l^{ADM} = \hat{\mathbf{R}}_{l-1}^{l} \cdots \hat{\mathbf{R}}_{f}^{1} r_f$;
while $\|r_l^{ADM}\|_\infty > Tol_1$ *and* $\|\delta x_l\|_\infty > Tol_2$ **do**
  Construct/Update fine-scale Jacobean ($\mathbf{J}_f$);
  Restrict fine-scale system:
  $\mathbf{J}_l^{ADM} = \hat{\mathbf{R}}_{l-1}^{l} \cdots \hat{\mathbf{R}}_{f}^{1} \mathbf{J}_f \hat{\mathbf{P}}_{1}^{f} \cdots \hat{\mathbf{P}}_{l}^{l-1}$
  Solve ADM system: $\mathbf{J}_l^{ADM} \delta x_l = -r_l^{ADM}$;
  Prolong ADM solution:
  $\delta x_f = \hat{\mathbf{P}}_{1}^{f} \cdots \hat{\mathbf{P}}_{l}^{l-1} \delta x_l$;
  Update fine-scale residual r_f;
  Restrict fine-scale residual:
  $r_l^{ADM} = \hat{\mathbf{R}}_{l-1}^{l} \cdots \hat{\mathbf{R}}_{f}^{1} r_f$;
end

Numerical experiments

The ADM method described in the previous section has been implemented in a Matlab research reservoir simulator that solves the system of equations in Eq. (1) for a two-phase ($N_\alpha = 2$) water-oil ($\alpha = w, o$) system with heterogeneous capillary functions. To test the accuracy of the ADM method, a 999 m $\times$ 999 m 2D reservoir is considered on which 99 $\times$ 99 fine-resolution grid cells are imposed. The base 10 logarithm of the permeability is shown in fig. 3, whereas the porosity is uniform and equal to 0.2. A five-spot injection pattern is considered, where one rate constrained water injector (injection rate of 0.001 $\frac{pv}{day}$) and four pressure constrained producers ($BHP = 10\,bar$) are present. All wells are treated according to the Peaceman well model (Peaceman, 1978) with a fixed well index equal to 2000. The simulations are run until 1 PVI of water has been injected in the reservoir (corresponding to 1000 days). Two scenarios of increasing complexity are considered. First, a simple water flooding test case that does not involve any capillary pressure is simulated. This is done both for favorable and unfavorable displacement conditions. Then, a Leverett's J-function (Leverett, 1941) is employed to generate multiple (heterogeneous) capillary curves. For both scenarios, quadratic relative permeability curves with endpoints equal to 1, and 0 irreducible wetting and non-wetting phase saturations are considered.

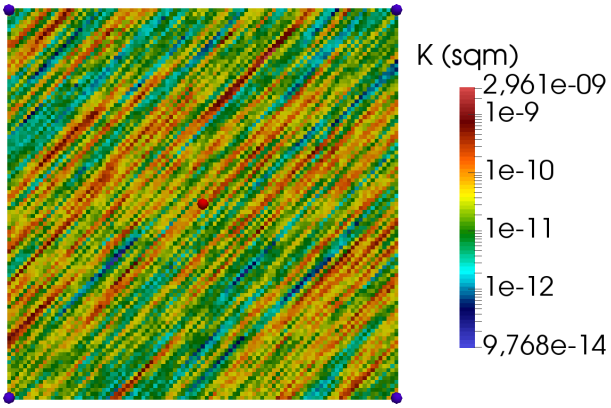

Figure 3 *Logarithm in base 10 of the permeability in m^2. The locations of the injector well (in red) and of the four producers (in blue) are also shown.*

Accuracy of the solution

To evaluate the accuracy of the ADM method its solution is compared against the one obtained with a fine-scale simulation. As a measure of the error in both primary variables,

$$\varepsilon_p = \underset{t=1}{\overset{N_{report}}{mean}} \left(\frac{\|p(t) - p_{ref}(t)\|_2}{\|p_{ref}(t)\|_2} \right) \tag{12}$$

is used for pressure, and

$$\varepsilon_S = \underset{t=1}{\overset{N_{report}}{mean}} \left(\frac{\|S(t) - S_{ref}(t)\|_2}{N_f} \right) \tag{13}$$

for saturation. Here, $p(t)$, $S(t)$, $p_{ref}(t)$ and $S_{ref}(t)$ are the pressure and saturation ADM and fine-scale solutions, respectively, at simulation time t. N_{report}, equal to 50 for the following test cases, is the number of simulation times for which the error is computed.

Case 1 - water flooding (no P_c)

Here, a water flooding problem without any capillary effect is solved both for unfavorable ($m = \frac{\mu_w}{\mu_o} = 0.1$) and favorable ($m = \frac{\mu_w}{\mu_o} = 10$) injection conditions. Figure 4 shows the fine-scale and the ADM saturation maps after injection of 0.5 PVI for both scenarios along with the absolute error of ADM with respect to the fine-scale ($|S - S_{ref}|$). Note that ADM provides an accurate solution for both scenarios. However, when a less viscous fluid is injected, the front is less sharp and viscous fingering is observed. As a consequence, compared with favorable scenario, capturing all interfaces requires ADM to employ more fine-scale grid blocks and a smaller coarsening criterion threshold has to be used in order to control the error. Fig 4 (c) shows that the error in the saturation solution is very low almost in the entire domain and only a few cells present an absolute error greater than 0.1. As shown in fig. 4 (f), when a more viscous fluid is injected, the error is very localized at the interface with values lower than 0.1 for all cells.

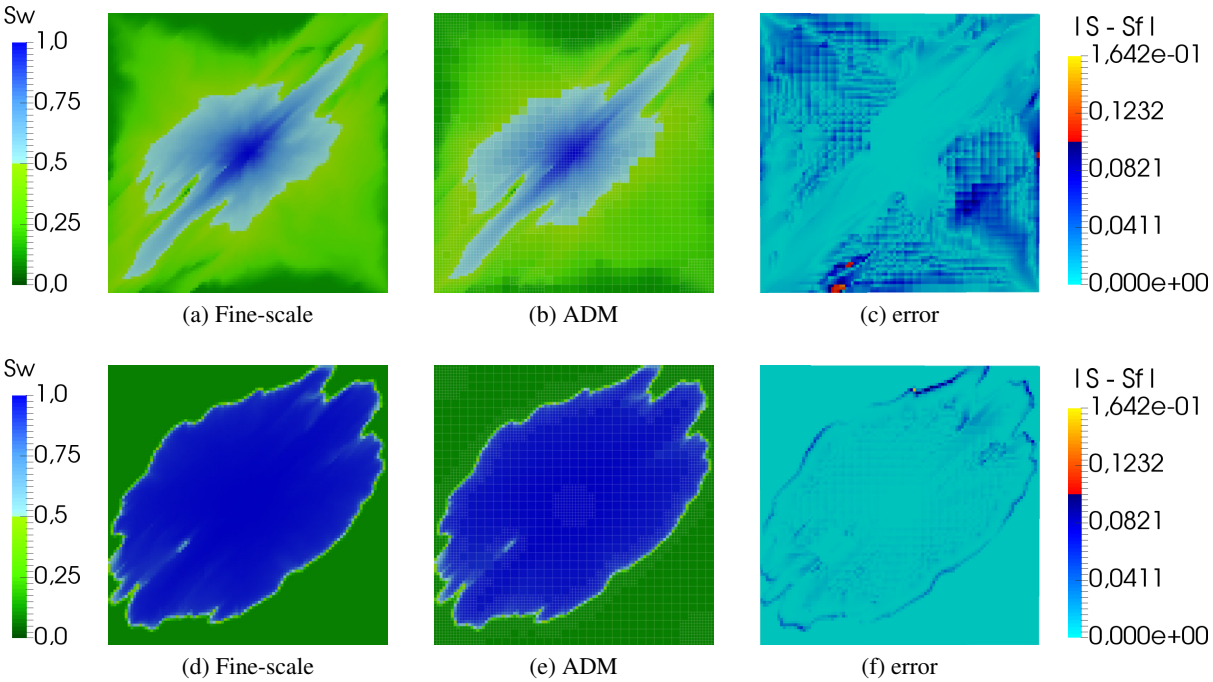

(a) Fine-scale (b) ADM (c) error

(d) Fine-scale (e) ADM (f) error

Figure 4 *Case 1 - fine-scale and ADM saturation maps after injection of 0.5 pv and absolute ADM error with respect to the fine-scale solution for both unfavorable (a - c) and favorable displacement (d - f).*

Fig. 5 shows the pressure and saturation errors for both injection scenarios as functions of the coarsening criterion threshold. For both cases reducing the coarsening threshold reduces the ADM error. However,

for the case of favorable displacement, the error reduction is less significant. This is due to the fact that the very sharp front is easily captured even with higher thresholds. It is also noticed that the unfavorable displacement, due to presence of fingers, is relatively more sensitive to the coarsening threshold used.

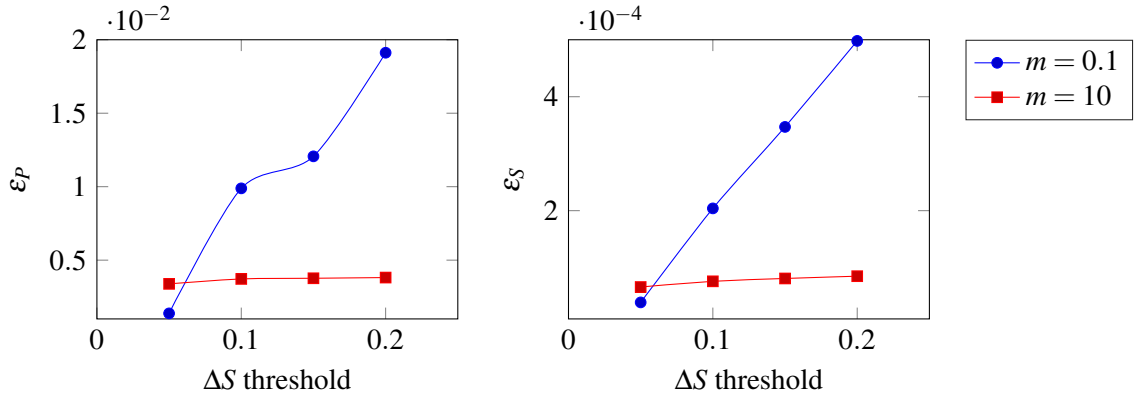

Figure 5 *Case 1 - ADM pressure and saturation errors as functions of the coarsening criterion threshold.*

Case 2 - Capillarity heterogeneities

As a second test case a water-flooding problem with a viscosity ratio $m = \mu_w/\mu_o = 0.667$ is considered. The capillary pressure curves read (Li, 2014)

$$P_c = P_o - P_w = 4.361 \cdot 10^{-2} \sqrt{\frac{\phi}{K}} J(S_w), \tag{14}$$

where

$$J(S_w) = 0.1 \left(\frac{1 - S_{wirr}}{S_w - S_{wirr}} \right)^{-0.5}. \tag{15}$$

Figure 6 (a) shows the capillary curves for the maximum and the minimum permeability values of the the reservoir of fig. 3. Figure 6 (b) shows the capillary pressure at the beginning of the simulation. Note that, since the initial water saturation is uniformly equal to 0.1, at the beginning of the simulation the capillary forces are not in equilibrium.

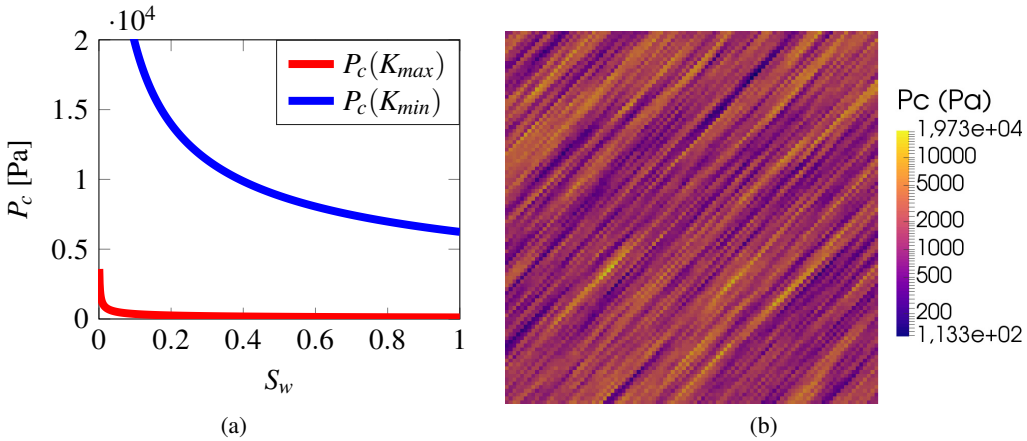

(a) (b)

Figure 6 *Capillary pressure: (a) shows the curves for the maximum and the minimum permeability values. (b) shows the capillary pressure distribution at the initial water saturation value of 0.1.*

Figure 7 shows fine-scale and ADM saturation maps after injection of 0.5 PVI along with the absolute error of ADM with respect to the fine-scale solution ($|S - S_{ref}|$). Note that water saturation front is

captured accurately by ADM even for this challenging scenario. Only a few cells present an absolute error greater than 0.1. For the remaining cells the error in the saturation solution is due to the averaged saturation value assigned to coarse blocks.

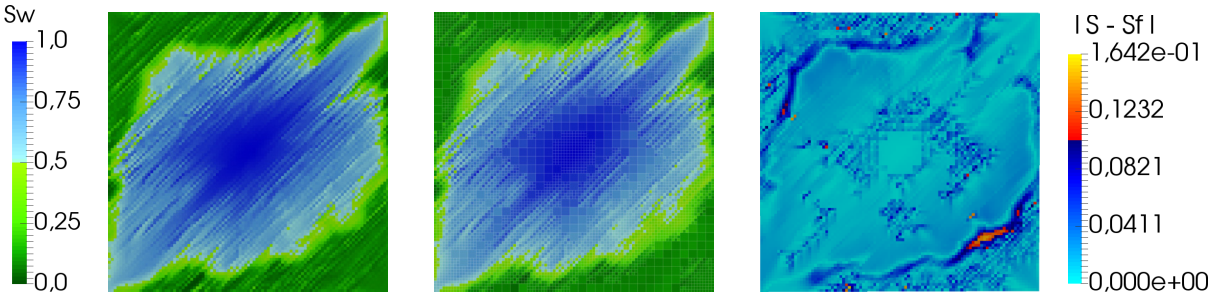

(a) Fine-scale (b) ADM (c) error

Figure 7 *Case 2 - saturation map after injection of 0.5 pv for fine-scale (a) and ADM simulation (b). The error in the ADM solution with respect to the reference is also shown (c).*

The averaged pressure and saturation errors, as functions of the coarsening threshold criterion, are shown in fig. 8. As for the previous test case a smaller threshold allows for a reduction of both the pressure and the saturation errors.

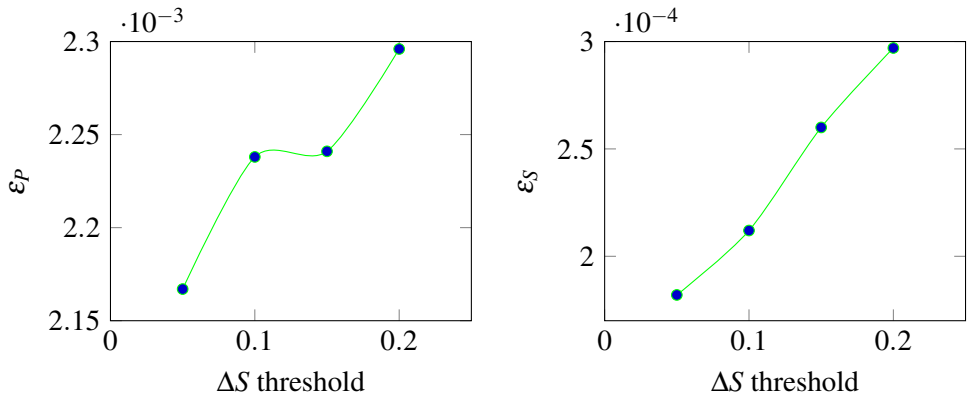

Figure 8 *Case 2 - ADM pressure and saturation errors as functions of the coarsening criterion threshold.*

Number of ADM grid blocks

The main objective of ADM is to obtain an accurate solution, without loosing fine-scale information (e.g. heterogeneity, interactions at smaller length scales), with less degrees of freedom than the fine-scale solver. Thus, it is important to analyze the performance of ADM in terms of number of nodes employed throughout the simulation. Figure 9 shows the history of the number of ADM grid-blocks red during the simulation, for the two test cases studied here. The coarsening criterion threshold for each scenario was chosen so that almost similar pressure and saturation errors were obtained for all cases. The values used were 0.1 for the unfavorable displacement water-flooding problem and 0.15 for the other two scenarios. Notice that all presented cases provide very accurate solutions compared with those obtained with a fine-scale simulator. For practical applications, however, one may employ looser tolerances for ADM as highly accurate representation of the fine-scale saturation map may not be required due to the uncertainties within the real-field data.

Conclusion

An Algebraic Dynamic Multilevel method for fully-implicit (and sequential-implicit) simulation of multiphase flow in heterogeneous porous media with non-linear heterogeneous capillary effects was presented. The FIM system is described on a dynamic multilevel grid resolution by the means of sequences

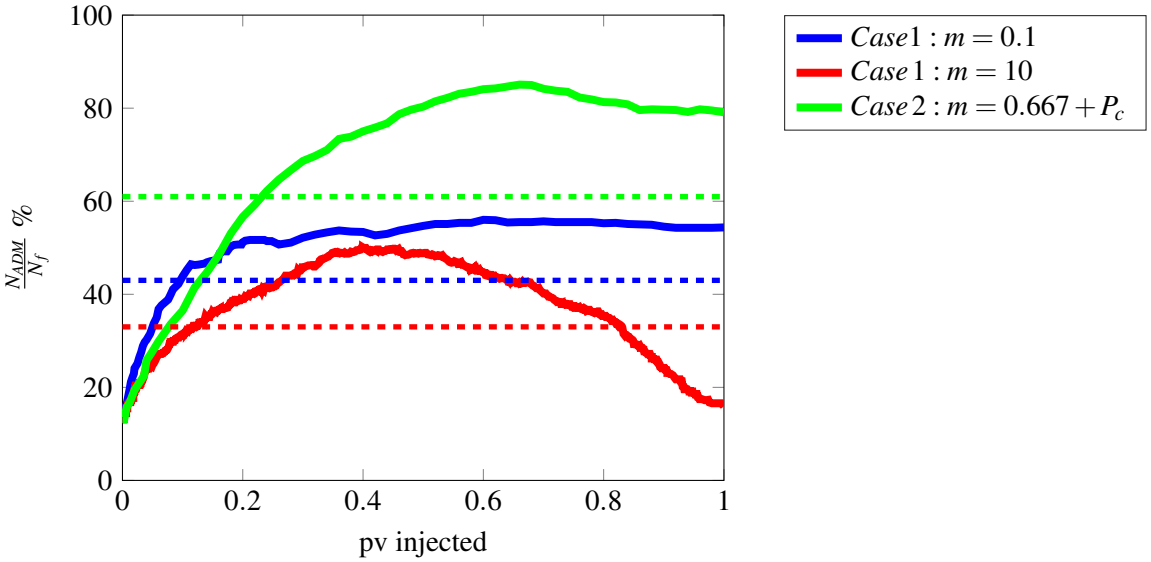

Figure 9 *Number of grid-blocks (as percentage of fine-scale cells) employed by ADM throughout the time-dependent simulations. The average values are represented by the dashed lines.*

of restriction and prolongation operators. Thus, fine-scale resolution is only employed where and when needed.

Numerical experiments show that ADM can accurately solve challenging (both in terms of rock and fluid properties) test cases employing only a fraction of the fine-scale grid blocks. The number of ADM grid blocks depends on the physics considered.

ADM combines advantages of DLGR techniques with those of multiscale methods. As such, it represents a potential important advancement for both. Ongoing research activities include the extension of ADM to more realistic scenarios where more complex fluid and rock physics are considered (e.g. compositional displacements and fractured media).

Acknowledgments

The authors thank Delft Advanced Reservoir Simulation (DARSim) research team for the fruitful discussions. This work was partly funded by Shell Global Solutions International B.V. (grant number: PT38338).

References

Bell, J. and Shubin, G. [1983] An adaptive grid finite difference method for conservation laws. *J. Comput. Phys.*, **52**, 569–591.

Berger, M. and Oliger, J. [1984] Adaptive mesh refinement for hyperbolic partial differential equations. *J. Comput. Phys.*, **53**, 484–512.

Boerrigter, P., de Zwart, A., van Batenburg, D., Bosch, M. and Vink, J. [2011] Application of dynamic gridding techniques to IOR/EOR-processes. *in: SPE Reservoir Simulation Symposium, 21-23 February, The Woodlands, Texas, USA, 2011, SPE paper 141711.*

Brown, H.W. [1951] Capillary pressure investigations. *Petroleum Transactions, AIME*, **192**, 67–74.

Chaouche, M., Rakotomalala, N., Salin, D., Xu, B. and Yortsos, Y. [1994] Capillary effects in drainage in heterogeneous porous media: continuum modelling, experiments and pore network simulations. *Chemical Engineering Science*, **49**, 2447–2466.

Cusini, M., van Kruijsdijk, C. and Hajibeygi, H. [2016] Algebraic dynamic multilevel (ADM) method for fully implicit simulations of multiphase flow in porous media. *J. Comput. Physics*, **314**, 60–79.

Edwards, M. and Christie, M. [1993] Dynamically adaptive Godunov schemes with renormalization in reservoir simulation. *in: SPE Symposium on Reservoir Simulation, 28 February-3 March, New Orleans, Louisiana, 1993, SPE paper 25268.*

Faigle, B., Helmig, R., Aavatsmark, I. and Flemisch, B. [2014] Efficient multiphysics modelling with adaptive grid refinement using a MPFA method. *Computat. Geosci.*, **18**, 625–636.

Hajibeygi, H. and Jenny, P. [2011] Adaptive iterative multiscale finite volume method. *J. Comput. Phys.*, **230**(3), 628–643.

Han, D., Yan, C. and Peng, L. [1987] A more flexible approach of dynamic local grid refinement for reservoir modeling. *SPE 16014, SPE Symposium on Reservoir Simulation, 1-4 February, San Antonio, Texas, USA, 1987.*

Heinemann, Z., Gerken, G. and von Hantelmann, G. [1983] Using Local Grid Refinement in a Multiple-Application Reservoir Simulator. *in: SPE Reservoir Simulation Symposium, 15-18 November, San Francisco, California, USA, 1983, SPE paper 12255.*

Helmig, R., Weiss, A. and Wohlmuth, B.I. [2007] Dynamic capillary effects in heterogeneous porous media. *Comput. Geosic.*, **11**, 261–274.

Homsy, G.M. [1987] Viscous fingering in porous media. *Annu. Rev. Fluid. Mech.*, **19**, 271–311.

Hoteit, H. and Chawathé, A. [2014] Making Field-Scale Chemical EOR Simulations a Practical Reality using Dynamic Gridding. *in: SPE EOR Conference at Oil and Gas West Asia, 31 March-2 April, Muscat, Oman, 2014, SPE paper 169688.*

Hou, T.Y. and Wu, X.H. [1997] A multiscale finite element method for elliptic problems in composite materials and porous media. *J. Comput. Phys.*, **134**, 169–189.

Jackson, M.D., Muggeridge, A.H., Mostaghimi, P., Kamali, F. and Pain, C.C. [2015] A dynamic mesh approach for simulation of immiscible viscous fingering. *in: SPE Reservoir Simulation Symposium, 23-25 February, Houston, Texas, USA, 2015, SPE paper 173281-MS.*

Jenny, P., Lee, S.H. and Tchelepi, H.A. [2003] Multi-scale finite-volume method for elliptic problems in subsurface flow simulation. *J. Comput. Phys.*, **187**, 47–67.

Kunze, R., Lunati, I. and Lee, S.H. [2013] A multilevel multiscale finite-volume method. *J. Comput. Phys.*, **225**, 502–520.

Leverett, M. [1941] Capillary behaviour in porous solids. *Transactions of the AIME*, **142**, 159–172.

Li, B. [2014] *Modeling geological CO2 sequestration:translations across spatial scales and advancements in nonlinear newton solver.* Phd thesis, Stanford university, USA.

Nilsson, J., Gerritsen, M. and Younis, R. [2005] A novel adaptive anisotropic grid framework for efficient reservoir simulation. *in: SPE Reservoir Simulation Symposium, 31 January-2 Feburary, The Woodlands, Texas, USA, 2005, SPE paper 93243.*

Pau, G.S.H., Bell, J.B., Almgren, A.S., Fagnan, K. and Lijewski, M.J. [2012] An adaptive mesh refinement algorithm for compressible two-phase flow in porous media. *Computat. Geosci.*, **16**, 577–592.

Peaceman, D.W. [1978] Interpretation of well-block pressures in numerical reservoir simulation. *SPE J.*, **18 (3)**, 183–194.

Schmidt, G. and Jacobs, F. [1988] Adaptive local grid refinement and multi-grid in numerical reservoir simulation. *J. Comput. Phys.*, **77**, 140–165.

Zhou, H., Lee, S. and Tchelepi, H. [2011] Multiscale finite-volume formulation for saturation equations. *SPE J.*, **17**, 198–211.